Angular intensity of nonequilibrium interfacial dynamic light scattering: Succinonitrile and naphthalene

L.M. Williams and H.Z. Cummins
Department of Physics, City College, CUNY, New York, New York 10031

L.O. Ladeira and O.N. Mesquita
Departamento de Fisica, Universidade Federal de Minas Gerais, Belo Horizonte 31270 Minas Gerais, Brazil
(Received 16 October 1991)

We have investigated the phenomenon of intense dynamic light scattering at the nonequilibrium crystal-melt interface in succinonitrile and naphthalene, in order to resolve the ongoing controversy over its origin. Of the several models that have been proposed to explain this phenomenon, the microbubble model of H.Z. Cummins *et al.* [Solid State Commun. **60**, 857 (1986)] and the mesophase model proposed by J. Bilgram and co-workers [P. Boni, J.H. Bilgram, and W. Kanzig, Phys. Rev. A **28**, 2953 (1983)] are the only two still considered to be consistent with most of the experimental observations. In these experiments the angular dependence of the scattered light was investigated. In the mesophase model the angular dependence of the scattered light is described by the Ornstein-Zernike form $I(q) = I_0(1 + q^2\xi^2)^{-1}$, whereas light scattered by bubbles can be modeled by the Mie scattering theory. The data for both materials were found to be incompatible with the Ornstein-Zernike form; but could be reasonably well fit by the Mie theory. The behavior of the onset of scattering was also investigated, and it was found that the product $R_0 t_0 v_g^2$ was a constant, where R_0 is the onset radius, t_0 the onset time, and v_g the crystal growth velocity. This result is consistent with the analysis of Mesquita *et al.* [Phys. Rev. B **38**, 1550 (1988)], in which the onset of the scattering was modeled by considering the rate of buildup of dissolved gas at the advancing crystal-melt interface. The time taken for the disappearance of the scattering after growth was terminated was also investigated. Lastly, the gases dissolved in our samples of succinonitrile were identified by mass spectroscopy and found to have a composition similar to air.

PACS number(s): 68.45.-v, 42.25.Fx, 78.35.+c, 81.10.Fq

I. INTRODUCTION

In 1978 the phenomenon of intense quasielastic light scattering at the growing crystal-melt interface was reported by Bilgram and co-workers [1,2]. This observation in the ice-water system revealed that the scattered light is characterized by an exponentially decaying correlation function of the form $c(t) =< I(0)I(t) >= B\left(1 + ae^{-\Gamma t}\right)$, with $\Gamma = 2Dq^2$, where q is the scattering vector and D is an effective diffusion constant. Since this initial observation, the phenomenon has been observed in a total of eight different materials, as shown in Table I, in experiments performed by Bilgram's group [1–9], Cummins's group [10–14], Yeh's group [15,16], Mesquita's group [17], and Toledano's group [18, 19]. For a comprehensive review of past experimental work see [20].

This scattering phenomenon has been shown to have the following basic properties.

(a) It occurs in a fluid boundary layer at least several micrometers in thickness, and in salol and benzophenone coexists with scattering due to translational dynamics seen on the crystal surface.

(b) It is much more intense than scattering from either the crystal surface or the bulk fluid.

(c) It requires an onset time on the order of hours to begin, which is increased by prolonged degasification of the sample.

(d) The intensity correlation function of the scattered light is approximately exponential with a polydispersity that varies in some experiments from a small value ~ 0.1 at onset to a value on the order of unity after prolonged growth.

(e) It occurs on both atomically smooth and rough interfaces.

(f) The effective diffusion constant D is typically 10^4 times smaller than the molecular self-diffusion coefficient, and 10^6 times smaller than the thermal diffusion coefficient of normal liquids.

(g) It can persist for many hours after growth has stopped.

(h) The scattering layer can lift off of the interface if the crystal is melted back quickly.

Several models have been proposed to explain the origin of this diffusive scattering [21, 22, 3]. However, most of the earlier models are now generally regarded as inconsistent with various elements of the experimental data, particularly the observed thickness of the scattering layer which increases with decreasing growth velocity. Thus currently the mesophase model proposed by Boni, Bilgram, and Kanzig [5] and subsequently modified by Steininger and Bilgram [9], and the gaseous microbubble model proposed by Cummins *et al.* [12], are the only extant models generally consistent with the properties (a)–(h) given above.

TABLE I. Diffusion coefficients and corresponding radii from boundary layer light scattering measurements.

Material	Diffusion coefficent (cm^2/s^{-1})	Radius (μm)	Ref.
Benzophenone	$\sim 1 \times 10^{-10}$	~ 2	a
Biphenyl	$4.9 \times 10^{-10} - 1.5 \times 10^{-9}$	1.0–3.6	17
Cyclohexane	6×10^{-9}	0.26	8
Cyclohexanol	$2 \times 10^{-11} - 9 \times 10^{-11}$	0.34–1.5	13
Naphthalene	$1.6 \times 10^{-10} - 1.3 \times 10^{-9}$	1.7–8.2	17
Salol			
a axis	$7.5 \times 10^{-10} - 1.25 \times 10^{-9}$	0.22–0.36	6
a axis	$0.6 \times 10^{-10} - 1.0 \times 10^{-10}$	2.7–4.6	11
b axis	$1.0 \times 10^{-10} - 1.0 \times 10^{-10}$	0.27–2.7	11
b axis	$2.3 \times 10^{-12} - 7.8 \times 10^{-10}$	0.35–117.0	14
Succinonitrile	$3.6 \times 10^{-10} - 4.5 \times 10^{-9}$	0.4–5.0	b
Succinonitrile	$1.5 \times 10^{-9} - 3.0 \times 10^{-9}$	0.6–1.2	18
Degased	$2.9 \times 10^{-11} - 6.9 \times 10^{-11}$	31.0–52	18
Water			
a-*c* axis	$1.5 \times 10^{-11} - 3.0 \times 10^{-9}$	0.3–65	16
c axis	$1.4 \times 10^{-8} - 5.7 \times 10^{-8}$	0.019–0.079	5
c axis	$4.5 \times 10^{-9} - 6.3 \times 10^{-9}$	0.059–0.072	16
D_2O	close to H_2O values		4

[a]O.N. Mesquita (unpublished).
[b]This work.

The explanation of the properties of the mesophase has evolved somewhat from its initial form given in Boni, Bilgram, and Kanzig [5]. The initial explanation stated that as the crystal grew a first-order phase transition took place at the interface, and a boundary layer formed between the solid and liquid phase characterized by a large isothermal compressibility χ_T (for the ice-water system 700 times that of normal water). This large value of χ_T would give rise to anomalously large entropy fluctuations that strongly scatter light, while the corresponding decrease in the thermal diffusion coefficient would cause the Rayleigh line to be very narrow compared to the normal liquid phase. However, recent measurements by Steininger and Bilgram [9] of the dependence of the linewidth Γ on the scattering vector $\mathbf{q}$ indicate that the scattering cannot arise from thermodynamic fluctuations in a pure one-component system, since one would expect to find a departure from the $\Gamma \propto q^2$ behavior for such a system when $q\xi \geq 1$; but no such departure is observed. Steininger and Bilgram noted that this result is in agreement with the predictions of Mazur and co-workers [21, 23], who have concluded that thermodynamic fluctuations cannot give rise to this diffusive scattering phenomenon. Thus the putative mesophase layer is now thought to consist of small weakly bound aggregates of molecules, and the corresponding fluctuations in the index of refraction are ascribed to the formation and decay of intermolecular structures. (We will discuss the mesophase model further in Sec. IV.)

In the microbubble model [12] the scattering is attributed to bubbles that form at the interface as gas dissolved in the melt is segregated by the growing crystal until the gas concentration at the interface passes the saturation concentration. The profile of the gas concentration in the melt can be calculated by solving the diffusion equation for the concentration $C(z,t)$ in the frame of reference of the moving interface:

$$\frac{\partial C}{\partial t} = v_g \frac{\partial C}{\partial z} + D\frac{\partial^2 C}{\partial z^2}, \tag{1.1}$$

where v_g is the growth velocity and D is the diffusion coefficient of the gas in the melt. For steady state the solution to Eq. (1.1) [12] is

$$C(z) = C_0\left(1 + \frac{1-k}{k}e^{-v_g z/D}\right), \tag{1.2}$$

where C_0 is the background concentration of gas in the melt and k is the segregation coefficient. Note that from Eq. (1.2) the thickness t_h of the high-concentration layer in the melt at steady state is given by $t_h = D/v_g$, i.e., the thickness of the layer increases with decreasing growth speed. The full time-dependent diffusion equation (1.1) has been solved by Pohl [24]. The approximate solution valid for small k is

$$\frac{C(z,t)}{C_0} = 1 + \frac{1-k}{k}\left(e^{-v_g z/D} - e^{-(v_g/D)(1-k)(z+kv_g t)}\right). \tag{1.3}$$

Thus the concentration at the interface $C_i(t) = C(z = 0, t)$ follows the time dependence

$$\frac{C_i(t)}{C_0} = 1 + \frac{1-k}{k}\left(1 - e^{v_g^2 \frac{(1-k)k}{D} t}\right). \quad (1.4)$$

We next consider a bubble of gas of radius R. If surface tension is neglected, then a bubble of *any* radius could exist in equilibrium with the fluid if the concentration C were exactly equal to the saturation concentration C_s. When surface tension is included, however, bubbles can only exist in (unstable) equilibrium if the liquid is supersaturated, i.e., if $f = C/C_s > 1$. If the fluid pressure is P_l and the surface tension is σ, bubbles can exist in (unstable) equilibrium only if $f = P_g/P_l = 1+(2\sigma/RP_l)$, where Henry's law has been assumed to apply (the equilibrium pressure of the gas in the bubble is linearly related to its concentration in the liquid). Thus we have

$$R_c = \frac{2\sigma}{[P_l(f-1)]}, \quad (1.5)$$

where P_l is assumed to be the vapor pressure of gas in equilibrium with a liquid having dissolved gas concentration C_s. Bubbles with $R < R_c$ will collapse, while those with $R > R_c$ will grow [25]. Equation (1.5) sets a concentration-dependent lower limit on the radius of bubbles that will nucleate.

If bubbles are assumed to nucleate by homogeneous nucleation then the nucleation rate J would be given by

$$J = Ae^{-\Delta F_c/k_B T}, \quad (1.6)$$

where the prefactor A depends on various material parameters and is typically $\sim 10^{32}$ [26]. The free-energy barrier height ΔF_c for formation of a bubble of critical radius R_c is given by

$$\Delta F_c = \frac{4}{3}\pi\sigma\ R_c^2 = \frac{16\pi\sigma^3}{3(P_g - P_l)^2}, \quad (1.7)$$

where σ is the interfacial tension, P_g is the gas pressure inside the bubble, and P_l is the hydrostatic pressure. If we assume that the bubbles are nucleated heterogeneously, which is almost certainly the case, Eq. (5) can be amended by inserting a factor ϕ which accounts for the reduction of the free energy of formation of bubbles by the heterogeneous nucleation mechanism

$$J = Ae^{-\phi\Delta F_c/k_B T}. \quad (1.8)$$

ϕ can be calculated for several simple geometries [27], but in general the precise form of ϕ is unknown. However, one can assume that $\phi \ll 1$.

There is substantial experimental evidence for the assumption that the crystal-melt interface considerably lowers the heterogeneous nucleation barrier for the formation of bubbles. In 1973, Wilcox and Kuo [26] summarized the extensive literature on the observation of the generation and trapping of gas bubbles in melt-grown crystals. They noted that bubble formation during the freezing of water is particularly well known, and that in 1870 Bunsen had obtained bubble-free ice for the first time by directional freezing downward of water boiled in the tube and then sealed to exclude air. The capture of gas bubbles during solidification of both water and salol has been observed and photographed extensively by Geguzin and Dzuba [28]. Gas-bubble trapping during crystal growth is also an important technical problem since it leads to voids and imperfections in crystals.

An important clue to the effect of crystal surfaces on gas-bubble nucleation was found by Hemmingsen and coworkers [29,30]. They studied bubble nucleation in water equilibrated with various gases at high pressure and then decompressed to atmospheric pressure. No nucleation was observed for initial pressures below 190 atm for N_2, or below 300 atm for He, but massive nucleation rates were observed for 20–30 atm higher initial supersaturation. When water was saturated with succinic acid or potassium nitrate and cooled to produce crystalline precipitates, it was found that the gaseous supersaturation threshold for bubble nucleation on the crystal surfaces was far lower than the value required for nucleation either in the bulk fluid or on the glass-liquid interface [30]. For succinic acid, the threshold (with Ar) was found to be less than 5 atm. It therefore seems likely that the free-energy barrier required to nucleate gas bubbles on the surface of a crystal is greatly decreased relative to the bulk value $\Delta F = \frac{4}{3}\pi\sigma R_c^2$.

Noting that the nucleation rate predicted by Eq. (1.8) decreases rapidly with increasing bubble radius suggests a mechanism in which the combined effects of Eqs. (1.8) and (1.5) can yield a narrow distribution of bubble sizes. As the crystal grows gas will be segregated at the interface and the concentration profile will develop at the interface. Once the concentration passes the saturation value C_s, then it is possible to nucleate bubbles; however, initially when $C = C_s$ the critical radius given by Eq. (1.5) is ∞, so the nucleation rate J predicted by Eq. (1.8) is zero. Thus the gas concentration will continue to increase until the critical radius predicted by Eq. (1.5) is small enough for Eq. (1.8) to predict an observable nucleation rate. If we further suppose that this minimum observable nucleation rate J is, e.g., $J = 10^3$ or J=1/(sec mm), utilizing Eq. (1.8) for the nucleation of 1-μm bubbles in salol, taking $A = 10^{32}$ [26], we have $\phi = 3.3 \times 10^{-6}$. Note, however, that when $R_0 = 2\mu$m, Eq. (1.8) gives $J \approx 10^{-84}$. Therefore no bubbles will appear until R_0 is very close to 1μm so that the combined effects of Eqs. (1.5) and (1.8) provide a very tight restriction on the initial bubble size. Therefore this mechanism predicts both an upper and a lower limit for the distribution of bubble sizes formed at onset. Of course the physical mechanism for such a small ϕ, and the way it varies with material properties is completely unknown, but Gilmer has suggested that wetting effects might play a crucial role [31].

If we linearize Eq. (1.4) and combine the result with Eq. (1.5), and also assume that the background concentration C_0 is equal to the saturation concentration C_s, then we find the following relationship between the onset radius R_0, onset time t_0, and the growth velocity v_g:

$$R_0 t_0 \approx \frac{2\sigma D}{P_l}\frac{1}{v_g 2}. \quad (1.9)$$

Experiments to test this relationship will be presented below.

There is now a substantial body of experimental evidence supporting the micro-bubble model. First, the model immediately explains the long onset time for scattering, since the buildup of gas concentration at the boundary, given by Eq. (1.4), is very slow at the small growth speeds employed in the experiments. Perhaps the strongest evidence is the direct observation of microbubbles included in solidified salol, after the scattering layer was trapped by the advancing crystal-melt interface [14]. Additional evidence comes from measurements of the dependence of the thickness of the scattering layer t_h on growth velocity in the ice-water system. Halter, Bilgram, and Kanzig [7] have measured t_h as function of growth velocity and seen that $t_h \propto v_g^{-1}$, in agreement with the predictions of the microbubble model for the width of the high gas concentration layer in the melt [see Eq. (1.2)]. Furthermore, Mesquita *et al.* [17] have analyzed the measurements of Boni, Bilgram, and Kanzig [5] of the increase in scattering intensity I and decrease in the linewidth Γ as scattering onsets. They have found that the data can be explained in terms of an increase in bubbles size, if the radius extracted from Γ is used to calculate $I(\theta)$ using the Mie scattering theory.

An additional aspect of the phenomenon that readily finds an explanation in the microbubble model is that upon rapidly remelting the crystal after scattering has begun, the scattering layer detaches from the surface of the crystal and floats in the melt. This detached scattering layer persists for some time, and gradually spreads out before disappearing. The "liftoff layer" can be easily understood as a consequence of the very small diffusion constants of the bubbles. This "liftoff" phenomenon has been observed in the ice-water experiments of both Vesenka and Yeh [16] and Halter, Bilgram, and Kanzig [7], and in experiments performed by Livescu *et al.* on cyclohexanol [13] and succinonitrile (observed during the course of the present work).

In the following sections we report measurements of the variation of the intensity of the scattered light with scattering angle. These experiments were motivated by prior measurements of $I(\theta)$ that led to continued controversy over the origin of the diffusive scattering. In 1986 Cummins *et al.* [12] measured $I(\theta)$ in salol and found that $I(\theta)$ decreased too rapidly with the scattering angle θ to be fit by the Ornstein-Zernike (OZ) function $I(\theta) = I_0(1 + q^2\xi^2)^{-1}$ that was predicted by the original mesophase theory, but could be reasonably described by the Mie theory. Contrary to this result, Steininger and Bilgram [8, 9] measured $I(\theta)$ in cyclohexane and found that $I(\theta)$ *could* be fit by the OZ function, but could not be fit by the Mie theory of scattering from spherical objects. In order to resolve this controversy we have performed two additional measurements of $I(\theta)$, on succinonitrile and naphthalene. In addition we will report measurements of the onset behavior of the scattering, and the persistence of the scattering after growth has been stopped. Finally, we describe an experiment in which mass spectroscopy was used to identify the gases dissolved in succinonitrile.

II. EXPERIMENTAL APPARATUS

A. Sample preparation

1. *Succinonitrile*

The material used was purchased from Fluka chemicals (99% purity). Succinonitrile ($C_4H_4N_2$) is a clear, nearly isotropic organic plastic crystal with a melting temperature of 58 °C. The refractive index of its melt is $n_m = 1.417$ [18], the viscosity at T=58 °C is $\eta = 0.026$P, and the molecular weight is 80.09 amu.

Succinonitrile grows with an atomically rough interface and is characterized by rapid growth kinetics which permits one to grow the crystal without starting with a seed crystal. It was possible to fill the cleaned sample cells with molten succinonitrile and, provided the sample was clean enough, after melting and slowly recrystallizing a suitable interface was formed when the sample was placed in the thermostat and a temperature gradient established. Several different grades of succinonitrile were used. Triply distilled material was sufficiently degassed to produce virtually *no scattering*. Therefore, for the onset measurements, singly distilled succinonitrile was used which produced the best compromise between elimination of dust contamination and retention of sufficient residual gas concentration to produce scattering. For the angular intensity measurements samples with a very high gas concentration were needed because it was found that at higher gas concentrations the size of the bubbles produced was smaller. To adequately differentiate between Mie scattering and Ornstein-Zernike scattering, a bubble radius in the range $0.2 < R < 0.6$ μm is required. Thus, for the angular intensity measurements, the sample tubes were loaded with undistilled succinonitrile and placed in the main apparatus in a zone refining configuration. The samples were then placed under vacuum and sealed. This loading procedure initially produced unsuitable samples because of dust contamination. The solidified sample was then melted back until only a small amount of crystal was left and was kept in the apparatus for about one month to allow the dust to settle to the bottom of the tube. The tube was then rapidly moved down in the temperature gradient which caused the interface to move up rapidly and trap the impurities in a layer near the bottom of the crystal. A good optical quality interface could then be established. Before each run we scanned the interface to check for any sign of scattering from residual dust, and only proceeded with the experiment if the interface was clean.

2. *Naphthalene*

Stock material purchased from Riedel de Haën (99% purity) was purified by vacuum sublimation. After purification, no light scattering was observed at growth velocities up to 2 μm/s; higher growth velocities produced unacceptable rounding of the interface.

Argon gas at 1 atm pressure was then bubbled through the purified material for $\sim$ 6 h, after which the typical

intense interfacial light scattering was observed. All results for naphthalene described in the following sections were obtained with this argon-treated material.

B. Light-scattering apparatus

The succinonitrile experiments were performed in the same light-scattering apparatus described in Ref. [14]. The lucite window and surrounding shield decribed in Ref. [14] was replaced by a single 10-cm-diam lucite cylinder of height 4 cm to improve the optical performance of the apparatus. For the naphthalene experiments the apparatus has been described previously in Ref. [17].

C. Mass-spectroscopy apparatus

The mass spectrometer used to analyze the residual gas dissolved in the succinonitrile samples was an Extranuclear C50 quadropole system (Extranuclear Inc. Pittsburgh, PA), equipped with a vacuum system consisting of a turbomolecular pump and a mechanical roughing pump. The gas analysis experiments were done in collaboration with Professor Robert Graff of the Chemical Engineering Department of CCNY, in his laboratory.

III. EXPERIMENTAL RESULTS

A. Angular intensity measurements

For both materials the scattered intensity $I(\theta)$ was measured with the incident polarization perpendicular to the scattering plane.

1. Succinonitrile

The sample was placed in the thermostat with a temperature gradient of about 20 °C/cm and grown at a velocity $v_g = 0.339$ μm/s. After about 3 h, when the scattering appeared to be uniform across the surface, we commenced taking data. The photomultiplier was rotated to the $\theta = 20°$ position and the first data point was taken. Each recorded point was the average of two 40-sec runs, where the total number of photocounts was counted using a Langley-Ford model 1096 correlator. For the $\theta = 20°$ point the incident laser intensity was adjusted to bring the total count to approximately 1.0×10^6 to enable us to easily compare different runs. Subsequent points were taken every 5° from 20° to 105°, the maximum angle possible with the apparatus. The data points were taken in a random sequence rather than sequentially to minimize the possibility of systematic error. After all the data were collected the scattering angles were corrected for the vertical components of the incident and scattered beam. The scattering angle θ is determined by $\cos\theta = \cos 2\psi \cos\theta_{PM} - \sin^2\psi$, where ψ is the angle between the incoming beam and the surface of the crystal (typically $\sim 8°$), and θ_{PM} is the angle through which the photomultiplier was rotated about the vertical axis of the sample tube relative to the incident beam direction. Prior to calculating θ, ψ was measured and corrected for refraction at the Plexiglas-air interface as the beam enters the thermostat.

In general, it is also necessary to correct for the θ dependence of the scattering volume. However, because the scattering layer is very thin, light scattered from the full scattering volume was collected by the optics at all scattering angles. This was established by observing the interface through the pinholes of the collection optics with a telescope.

In Fig. 1 we plot the results of a measurement of the angular intensity $I(\theta)$ in succinonitrile. The solid line represents a fit of the data with the Mie theory. A program was written that generates the Mie function for a Gaussian distributions of bubble scatterers based on a Mie function program generously provided by Barber of Clarkson University. Angular scattering functions were generated for various combinations of mean radius R_{av} and standard deviation θ_R and compared to the data. The solid line shown in Fig. 1 represents the nearest match found, and corresponds to a mean radius $R_{av} = 475$ nm and standard deviation $\theta_R = 47.5$ nm. (The radius extracted from dynamic light-scattering measurements was R$\sim$ 430 nm.) The dashed line represents the closest possible fit of the data with the Ornstein-Zernike theory. Curves of $I(\theta) = I_0[1 + q^2(\theta)\xi^2]^{-1}$ were generated for various values of ξ. For all values of ξ, the predicted $I(\theta)$ falls off too slowly with increasing θ to enable the data to be well fitted [note that reducing ξ to any finite value makes $I(\theta)$ fall off more slowly]. Both theoretical curves are normalized to 1.0×10^6 at $\theta = 26°$. From this figure it is quite clear that the Mie theory provides a much closer match to the succinonitrile data than the Ornstein-Zernike theory.

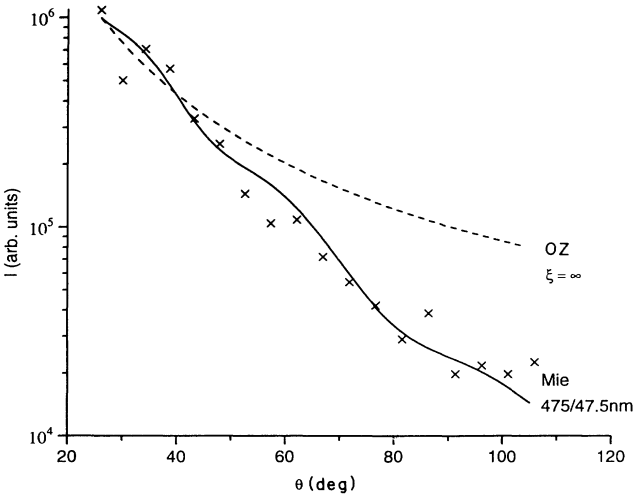

FIG. 1. Scattered intensity I vs angle θ for light scattered from the interface of a growing succinonitrile crystal. The solid line corresponds to the Mie curve for a Gaussian distribution of spherical scatterers of mean radius 475 nm and standard deviation 47.5 nm. The dashed line corresponds to the Ornstein-Zernike function for $\xi = \infty$. Both curves are normalized to 10^6 at θ=26°. The radius extracted from dynamic light-scattering measurements was $R \sim 430$ nm.

2. *Naphthalene*

For naphthalene the procedure was essentially the same. However, the range of angles over which data could be collected was limited to $25° \leq \theta \leq 60°$.

Only when the interface was without visible grain boundaries and analysis of the correlation function of the scattered light gave polydispersities less than 0.15 did we obtain reproducible intensity measurements. In Fig. 2 we plot the $I(\theta)$ results for the naphthalene measurement at a growth velocity of 0.25 μm/sec. (The continuous curve through the data points is a guide for the eye.) The average radius obtained from the dynamic light-scattering measurements was R=1.4 μm. Even though our range of angles is quite restricted, the peak observed near 50° was reproducible.

In Fig. 2 we have plotted (a) the Ornstein-Zernike $I(\theta)$ and (b) the Mie prediction, both normalized to match the data at $\theta = 25°$. The Ornstein-Zernike curve is for $\xi = 1.4$ μm. The closest Mie function to the experimental data was found for uniform bubbles of 1 μm radius. Note that this value of R, which provides a reasonable approximation to the experimental data, is somewhat below the value of R=1.4 μm found from the correlation functions. Although neither the Mie nor the Ornstein-Zernike curves fit the data well, the reproducible presence of a peak around the position of the peak in the Mie curve is indicative of Mie scattering. Furthermore, the occurrence of *any* peak whatsoever rules out the possibility that the data can be fit by Ornstein-Zernike theory which predicts that $I(\theta)$ should be a monotonically decreasing function of q.

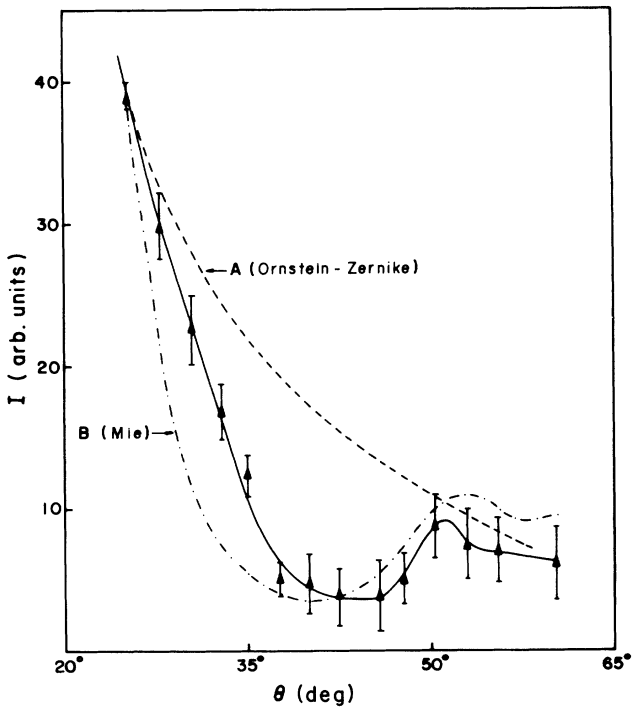

FIG. 2. Scattered intensity I vs scattering angle θ for light scattered from the crystal-melt interface of growing naphthalene saturated with argon at 1 atm. The continuous curve is a guide for the eye through the experimental data. Curve A is the Ornstein-Zernike function for $\xi = 1.4$ μm. Curve B is the Mie function for gas bubbles of radius 1 μm in liquid naphthalene. The hydrodynamic radius of the gas bubbles obtained by the dynamic light scattering was 1.4 μm.

B. Onset measurements

It is well established that diffusive scattering does not begin immediately when the crystal starts growing; there is always an onset time before scattering is observed. It has also been noted that the radius obtained from photon correlation spectroscopy is usually fairly constant for a particular sample from run to run. Note that for bubbles, the radius R is related to the effective diffusion constant D by $D = k_B T/4\pi\eta R$. The factor 1/4 (rather than the more familiar 1/6) results from the boundary condition for two-fluid motion, of no relative motion at the interface. Mesquita *et al.* [17] previously tested the onset relationship of Eq. (1.9) and found it to hold for naphthalene and biphenyl. Furthermore, they found a clear relation between onset radius R_0 and growth velocity v_g. However, when Lahererre *et al.* [19] investigated the onset behavior for succinonitrile they found no systematic variation in R_0, although they did find that the onset behavior could be described by Eq. (1.9). In our measurements we have investigated the dependence of the onset time t_0 and radius R_0 on growth velocity in both naphthalene and succinonitrile.

The succinonitrile measurements were performed with a temperature gradient of $\sim 20\,°\mathrm{C/cm}$, while in the naphthalene experiments the gradient was $\sim 6\,°\mathrm{C/cm}$. For naphthalene the growth velocities used varied from 0.15 to 0.5 μm/s; for succinonitrile from 0.212 to 2.217 μm/s. Each crystal was grown until a good quality interface was obtained. The sample was then left for a few days to allow any gases that had built up near the interface to diffuse away. The velocity was then selected, and growth was started. The interface was then observed visually. The first appearance of visible scattering usually corresponds to the signal detected by the photomultiplier tube being roughly twice the background signal of the light being scattered by the bulk melt. Once scattering was visible the onset time t_0 was recorded, and several correlation functions were then taken to determine R_0.

For naphthalene we plot $t_0 R_0$ vs v_g^{-2} in Fig. 3. The linear dependence predicted by Eq. (1.9) was confirmed. From the slope of the straight line we obtained $2\sigma D/P_l = (1.2 \pm 0.1) \times 10^{-9}\mathrm{cm}^3/\mathrm{s}$. With σ=29 erg/cm^2 and $P_l = 10^6$ dyn/cm^2 we obtain an estimate of $D = 2 \times 10^{-5}$ cm^2/s for the diffusion coefficient of argon in naphthalene.

The previously observed dependence of onset radius on growth velocity [17] was also observed in this material as shown in Fig. 4. Curve 1 is for naphthalene before purification with an unknown concentration of gas impurity and curve 2 is for purified naphthalene after saturation with 1 atm of pure argon. Within experimental error $R_0 \propto v_g^{-1}$.

For the succinonitrile data, in Fig. 5 we plot t_0 vs v_g^{-2}.

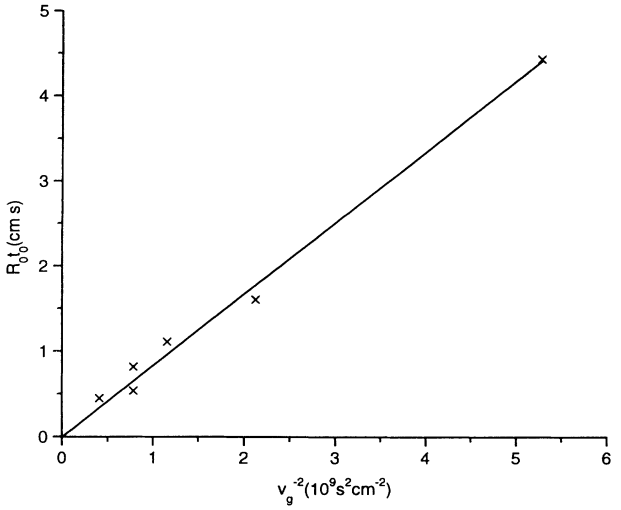

FIG. 3. Onset time t_0 for the appearance of light scattering from the crystal-melt interface of growing naphthalene saturated with argon times the onset radius R_0 of the gas bubbles as a function of v_g^{-2}. The dots are the experimental data and the continuous line is a linear regression fit to the data.

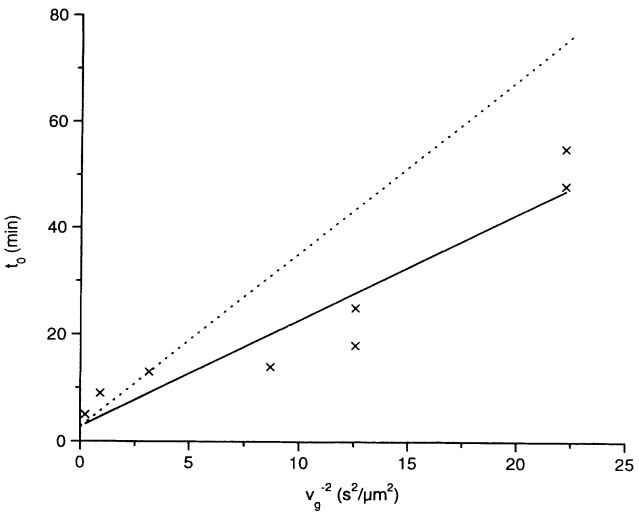

FIG. 5. Time for the onset of scattering t_0 (in minutes) vs the inverse square of the growth velocity (v_g^{-2}). The solid line represents a linear fit to the data. The dashed line represents a linear fit to the data of Laherrere *et al.*

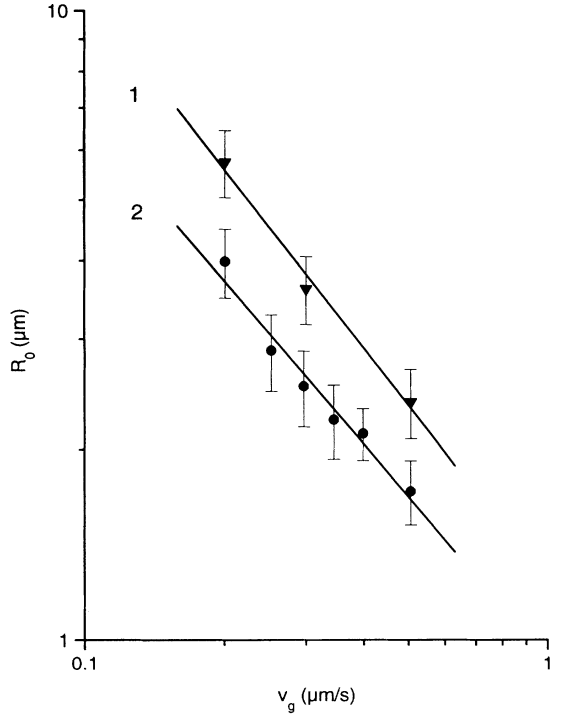

FIG. 4. Onset radius R_0 of the gas bubbles for growing naphthalene as a function of growth velocity v_g. The upper data points (triangles) were obtained with nonpurified naphthalene where the amount of gaseous impurity was unknown. The lower data points (circles) were obtained for naphthalene purified by sublimation, saturated with argon at 1 atm. Curves 1 and 2 are power-law fits to the data indicating that within experimental error $R_0 \propto v_g^{-1}$.

The solid line is a linear fit to the data. On the same graph we plot a linear fit to the data of Lahererre *et al.* [19]. We find that the data follow the behavior predicted by Eq. (1.9). We notice a positive intercept on the time axis of $\sim$ 3 min, which we interpret as a result of the time lag between the crystal pulling motor starting, and the interface reaching the steady-state undercooling necessary to achieve a growth velocity of v_g. However, in contrast to the naphthalene measurement but in agreement with the succinonitrile measurements of Lahererre *et al.* [19], we saw no systematic variation in R_0. In our succinonitrile experiments $R_0 \sim 4$ μm; in the experiments of Lahererre *et al.*, $R_0 \sim 1.1$ μm.

From Fig. 5 we note that our onset times were comparable to those Laherrere *et al.* obtained even though our onset radius was approximately four times larger. Equation (1.9) then implies that P_l (and therefore C_0) for our sample was smaller than theirs. These differences may be due to the different ways in which the samples were prepared. The sample of Laherrere *et al.* was not distilled, but zone refined many times. Our sample was distilled but not zone refined. It is quite possible that the gas may not be efficiently segregated by zone refining, or that once it is segregated it may redissolve in the solid. However, it is well known that vacuum distillation is a common, if not perfect, way of degasing materials. Thus it is quite probable that distilled samples have lower gas concentrations than zone refined samples. This is consistent with our experience with both succinonitrile and naphthalene, that if samples are either multiply vacuum distilled or vacuum sublimed the diffusive scattering phenomenon disappears.

The variation in onset radius between samples of the same material may alternatively have its origin in the heterogeneous nucleation process. It is also possible that different samples may have slightly different impurities

that, on a microscopic level, alter the number and nature of the heterogeneous nucleation sites at the interface. This may lower the nucleation barrier for some samples more than others, and lead to a variation in the onset behavior of the samples.

The observation that the onset radius changes with growth velocity in one experiment and does not in the other is somewhat harder to explain. One possible explanation is that the polydispersity of the succinonitrile system (0.35) was greater than the naphthalene system (0.15), and thus the wider distribution of bubble sizes in the succinonitrile system masks any systematic variation in the behavior of the onset radius.

C. Persistence of scattering after crystal growth has stopped

After turning off the growth drive motor we still observe light scattering in naphthalene for up to a few days, depending upon the velocity at which the crystal was growing. In salol and cyclohexanol, the persistence of scattering after the growth was stopped was attributed to the slow diffusion of the bubbles, which would then remain in the scattering volume for a long time [13]. In naphthalene, however, if we take account of the buoyancy and thermocapillary forces, all the bubbles should disappear from the scattering volume within a few minutes.

We found that the time t_d for disappearance of the scattering in naphthalene after the growth was stopped varied as $t_d \propto v_g^{-2}$, as shown in Fig. 6. Notice that for the lowest velocity we observed persistent scattering for about 72 h. The criterion used to determine that the scattering had terminated was that, even for an accumulation time of 10 min, no measurable correlation function could be obtained. In Fig. 7, we show the average radius of bubbles in naphthalene as a function of time after growth was stopped (the growth velocity in this experiment was 0.17 μm/sec). The data indicate that the bubble radius increases monotonically with time long after growth has stopped.

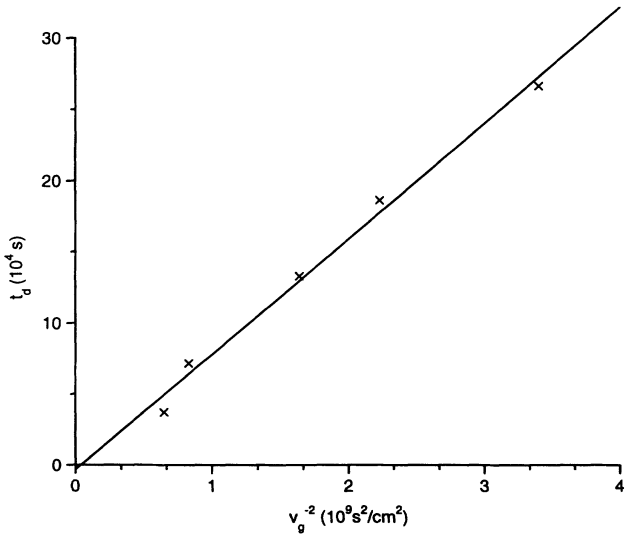

FIG. 6. Time t_d for disappearance of the light scattering at the crystal-melt interface of naphthalene saturated with argon, after the growth was stopped, as a function of v_g^{-2}; v_g is the growth velocity at which the crystal was growing before stopping it. The dots are the experimental data and the continuous line is a linear regression fit to the data.

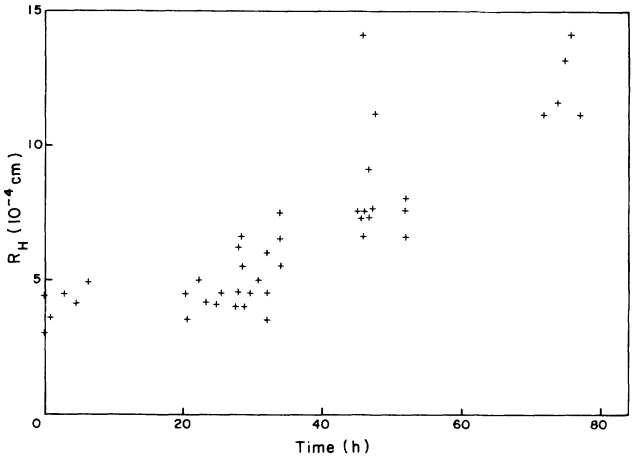

FIG. 7. Radius R of the gas bubbles obtained from dynamic light scattering at the crystal-melt interface of naphthalene saturated with argon as a function of time after the growth has been stopped. The growth velocity before stopping the growth was 0.17 μm/s.

The persistence of scattering after crystal growth has stopped can be understood by analyzing the time evolution of the dissolved gas concentration $C(z,t)$. If the concentration is sufficiently far above the saturation level when growth stops, and if decay by ordinary diffusion is sufficiently slow, new bubbles may nucleate (and existing bubbles may grow) until the supersaturation decreases to some threshold value.

To solve this problem we have to know the concentration profile just before the growth was stopped. If one starts with the diffusion equation in the frame of reference of the moving interface [Eq. (1.1)] but instead of the usual boundary condition $J_i = (1-k)v_g C_i$ for the gas flux into the liquid, we write $J_i = (1-k)v_g C_i - AC_i$, where the $-AC_i$ term corresponds to the gas flux spent to nucleate the gas bubbles, we see that in the steady-state regime we still get an exponentially decaying concentration profile as a function of the distance from the interface:

$$\frac{C(0,\infty)}{C_0} = 1 + \frac{(1-k)v_g - A}{kv_g + A} e^{-v_g z/D}. \tag{3.1}$$

[A similar profile is obtained if we use $J_i = (1-k)v_g C_i - B$, but the constant multiplying $e^{-v_g z/D}$ is different.] We can therefore take an initial profile for the concentration of $C(z,0) - C_0 = e^{-v_g z/D}$, and let it relax following the stationary diffusion equation:

$$\frac{\partial c}{\partial t} = D\frac{\partial^2 c}{\partial z^2} \tag{3.2}$$

with appropriate reflective boundary conditions at the

interface. The solution to this problem involves error functions; an approximate solution for the concentration at the interface is given by

$$C_i - C_0 \propto e^{v_g^2 t/D} \mathrm{erfc}\left[\left(\frac{v_g^2 t}{D}\right)^{1/2}\right]. \quad (3.3)$$

In this case, the scaling law $v_g^2 t_d/D \sim$ const would be valid if one assumes that the bubbles disappear when the supersaturation is always the same fraction of the initial supersaturation for all velocities. Therefore the slope of a plot of t_d vs v_g^{-2} should be proportional to the diffusion constant D. The slope of the straight line in Fig. 6 is 8×10^{-5} cm^2/sec, which is about four times larger than the diffusion coefficient of argon in naphthalene estimated from the onset measurements discussed above. The calculation here concerns the relaxation of the initial dissolved gas concentration profile by diffusion. It does not include the depletion of the gas layer by the formation of bubbles, for which case the problem would be intractible. It is important to mention that this experiment only gives reproducible results if the crystal has been grown long enough for the concentration field to achieve a steady-state profile.

D. Identification of gases dissolved in succinonitrile

A sample of succinonitrile (99% purity obtained from Fluka) was melted at atmospheric pressure and placed in an "Airfree" storage-reaction tube (Chemglass, Vineland, NJ model No. AF-0096-02). This tube is equipped with a "Chem-cap" high vacuum Teflon valve designed for use down to 10^{-7} Torr. The tube was connected to the mass spectrometer via a 1/4-in. swagelok fitting. The succinonitrile was allowed to solidify, and the tube was connected to the mass spectrometer. The Teflon valve was opened, and the gas collection tube was evacuated with a roughing pump. The tube was further evacuated through the mass spectrometer using its internal pump, and a spectrum was taken of the solid succinonitrile. The Teflon valve was then closed and the succinonitrile was melted by immersing the gas collection tube in water at 80 °C. At this stage many bubbles could be seen emerging from the liquid. After the succinonitrile was completely melted it was resolidified by immersing the gas collection tube in water at room temperature. The Teflon valve was opened again and another spectrum was taken. The two spectra were then subtracted to obtain the spectrum of the gas released by the bubbles. The subtracted spectrum is shown in Fig. 8(a), and magnified ten times in Fig. 8(b). The main peaks, in order of decreasing size, and the gases we attribute them to are given in Table II.

In the subtracted spectrum the succinonitrile peaks at 54 and 80 mass units present in the initial spectrum are no longer present. This is a useful check that the sensitivity of the spectrometer did not change between taking the first two spectra. From the figure we can see that the main gases released from the succinonitrile have an

TABLE II. Position of main peaks in the mass spectrum of Figs. 8(a) and 8(b) along with the corresponding intensities and probable origin. Numbers in parentheses are the atomic masses rounded to the nearest integer value.

Location of peak	Peak height	Identification (mass)
27.95	9834	N_2 (28)
31.80	1562	O_2 (32)
13.95	824	N (14)
17.90	775	H_2O (18)
16.95	178	OH^- (17)
16.00	164	O (16)
39.75	109	Ar (40)
43.80	24	CO_2 (44)
19.90	22	Ne (20)

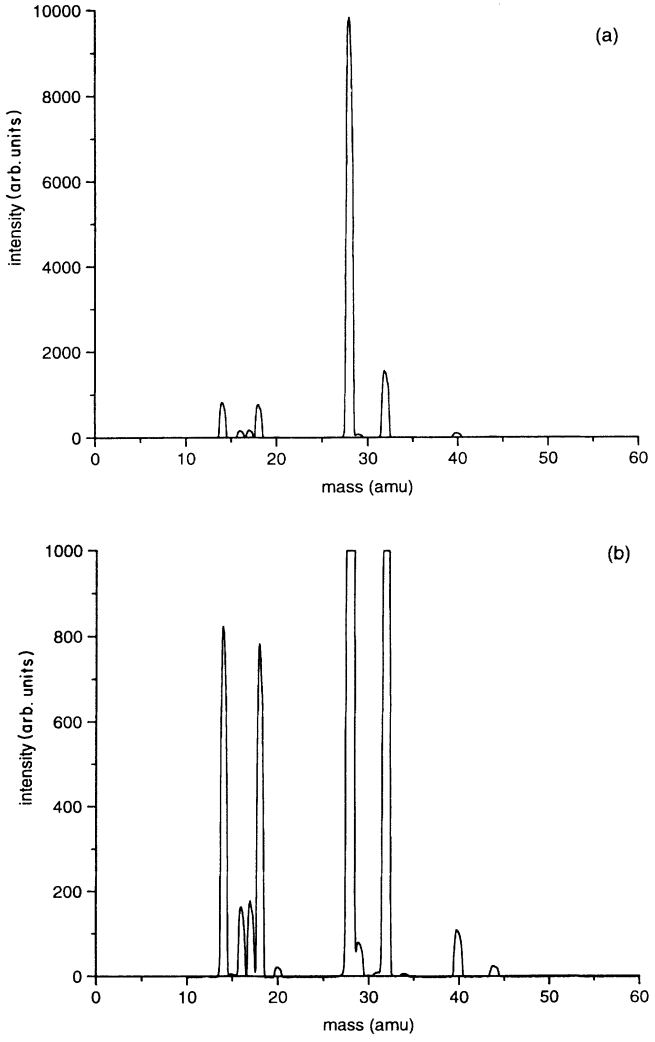

FIG. 8. (a) Mass-spectrometry data obtained by subtracting the spectrum of the solidified succinonitrile sample before the gases were released from the spectrum after the dissolved gases have been released. (b) The spectrum of (a) with the intensity axis magnified ten times to show detail.

essentially airlike composition. When this spectrum was compared to a spectrum of air, there was a slight difference in the ratios of the peak heights which can be attributed to the different solubilities of the various components of air in succinonitrile.

Laherrere *et al.* [19] reported that the gaseous impurity that causes the segregation of bubbles at the interface of succinonitrile is methanol. We found no significant evidence for methanol in our spectra. We compared our spectrum with a spectrum of air with a small amount of methanol impurity. A signature of the presence of methanol is a peak at ~31; there is no significant peak at 31 in our subtracted spectrum. Thus we conclude that for our succinonitrile methanol is not a major gaseous impurity, although, it may be present in the succinonitrile used by Laherrere *et al.* That the main gaseous impurity is something as commonplace as air is quite reasonable as the dynamic scattering at the interface seems to be an almost universal phenomenon in crystal growth.

IV. DISCUSSION AND CONCLUSIONS

The microbubble model explanation of the origin of diffusive scattering at the crystal-melt interface has several attractive features. It provides a mechanism for generating scatterers (bubbles) at the interface that have a reasonably narrow size distribution. The diffusive motion of the bubbles provides an explanation for the observed exponential correlation function of the scattered light. It also explains the long onset time for the scattering, since the buildup of excess dissolved gas concentration at the interface is a slow process at the low growth speeds employed. The narrowness of the scattering layer and its inverse dependence on growth velocity is explained by the exponential decay of the gas concentration with distance from the interface as predicted by Eq. (1.2). It also suggests why the observed effective diffusion coefficient D and polydispersity Q vary slightly from system to system, since the balance of transport and solute rejection and the nature of the heterogeneous nucleation process would both be expected to change from sample to sample.

There is much experimental evidence to support the microbubble model. In addition to the experiments reported on in this work, and the previously mentioned experiments, our group has shown that by prolonged pumping on the sample the scattering can be made to disappear [14]. Laherrere *et al.* [18] have shown that after repeatedly melting, recrystallizing, and pumping on their succinonitrile sample the scattering intensity decreased dramatically, and the bubble size increased. In an experiment that is somewhat the converse of these, Vesenka and Yeh [16] have shown that injecting helium into the melt strongly enhances the scattering. They have also shown that the bubble size decreases with positive gas pressure.

Also we note the observation that the scattering does not occur in materials that are very carefully purified by either vacuum distillation or vacuum sublimation, indicates that the phenomenon is an impurity effect of some sort.

In the course of recent preliminary experiments on cyclohexane in this laboratory, we have noted that this material has a tremendous affinity to dissolve gas. Stock material filtered through 0.2-μm filters and then used for crystal-growth experiments forms many large gas bubbles at the interface. Steininger and Bilgram [9] degas their material by repeatedly melting and recrystallizing it under a vacuum. However, even after this procedure they report that gas bubbles large enough to be seen by eye form at the interface once the material is introduced into the zone refining apparatus. Their material was then zone refined and the large easily visible bubbles disappeared. From our experience, however, it seems unlikely that this zone refining would reduce the background gas concentration in the sample to very low levels. In the experiments of Lahererre *et al.* [18] the succinonitrile used for the experiments was also multiply zone refined, yet the material produced strong scattering which was reduced in intensity by subsequently pumping on the system. Thus any mesophase scattering phenomena that occurs at the interface in cyclohexane prepared by zone refining would have to coexist with gaseous microbubbles that form when the remaining gas is segregated during the course of the subsequent experiments. It would be of considerable interest to perform experiments with cyclohexane prepared by vacuum sublimation or distillation to see if the scattering phenomena would disappear.

It has also been suggested that there may be more than one diffusive scattering phenomenon involved. Mazur and Keizer [23], and Vesenka and Yeh [16], have noted that the bubble sizes ($R \sim 0.025$ μm) obtained in the experiments by Bilgram's group [1–3, 5, 7] on the c axis of the ice-water system are considerably smaller than for all the other systems studied ($R_0 \sim 0.1 - 1.0\mu$m). This observation led them to conjecture that there might be two different scattering phenomena involved, one for the c face of ice, and microbubbles for all other systems. We note, however, that the observation of the "liftoff layer" [7], and the $1/v_g$ dependence of the thickness of the scattering layer [7], along with the fit of Mesquita *et al.* [17] using the Mie theory to the "I vs Γ" onset data of Boni, Bilgram, and Kanzig [5] all seem to suggest that the phenomenon present in the ice-water system is also microbubbles. It is possible that the origin of the small bubble size seen in the experiments of Bilgram's group may be related to the method of sample preparation. Thus it is interesting to contrast the sample preparation procedure of Bilgram's group with that of Brown *et al.* [15], who reported a larger bubble size in their ice-water experiments.

The procedure used by Bilgram's group is described in Ref. [3]. It is stated that the water is circulated through a Millipore system consisting of an organic adsorption filter, an ion exchanger and a mechanical filter with a 0.22-μm Millitube cartridge, until the resistivity of the water is below $10^{-7}\Omega$ cm^{-1} at 25 °C. This water is then used to make the seed crystal, and sample which is subsequently multiply zone refined. This procedure will indeed produce very pure water, but will probably not eliminate dissolved gases very efficiently. Thus it is quite likely that a sample prepared this way (i.e., with deionized water)

will contain more gas than a sample that has been multiply distilled. Furthermore, our experiments and those of Laherrere *et al.* [18] suggest that samples with a higher initial gas concentration C_0 produce smaller bubbles.

The cleanliness of the sample may also be a contributing factor. It is a well-known fact that if all sources of nucleation sites are removed or minimized, then liquids can withstand large supersaturations of gases before bubbles will nucleate. A related phenomenon is that of explosive boiling where a liquid is superheated past its boiling point but will not nucleate into a gas phase because of the unavailability of nucleation sites. Eventually the elevated threshold for nucleation is reached and the liquid explodes violently into the gas phase. One can imagine that as a sample is progressively cleaned its threshold concentration for heterogeneous nucleation C_N will rise until a state is reached where no sites are available, and C_N will equal the threshold for homogeneous nucleation. Wilcox and Kuo [26] have calculated both the necessary supersaturation and the critical radius for homogeneous nucleation of air in water. The critical radius is ~ 10 Å, and thus even the experiments of Bilgram's group are still far in the heterogeneous regime. Bilgram's group imposes strict criteria on each sample before data is taken [3]. These include an absence of dust in the water and an absence of bright spots caused by dust on the interface. However, in the experiments of Brown *et al.* [15], even though the samples are triply distilled, a region of the interface has to be chosen that is free of dust to perform the experiment. This implies that heterogeneous nucleation sites are pervasive on the interface. Thus the combination of a lower initial gas concentration with an environment more favorable to heterogeneous nucleation seems to yield a larger bubble size. In a subsequent publication, Vesenka and Yeh [16] noted a decrease in bubble size ($\sim 50 - 75$ nm) when the purification apparatus was moved inside of a helium filled work box in which the sample can be kept dust free. In the same publication Vesenka and Yeh injected the sample with helium, a procedure that will surely increase the background concentration of gas, but will also probably increase the amount of small particulate impurities. A large increase in scattering intensity but no decrease in bubble size was seen. Thus a large gas concentration alone cannot yield a small onset radius if an interface favorable to nucleation prevents the gas concentration from building up too much. Thus the uniquely small bubble radius observed in the ice-water system is probably a consequence of the ability of Bilgram's group to apply rigorous purification procedures (i.e., filtering, passing through ion-exchange columns) to the preparation of samples without having to resort to extensive distillation which removes gas.

Recently, Steininger and Bilgram have also conjectured that there may be two forms of diffusive scattering. They have suggested that for systems where the polydispersity index Q extracted from the light-scattering measurements is greater than 0.15 the scattering could be caused by bubbles, but for systems for which $Q = 0.15$ or less the scattering is caused by the mesophase boundary layer. For their measurements on cyclohexane $Q = 0.15$. However, we note that for our naphthalene sample $Q = 0.15$. Since our experiments indicate that the scattering in this material is due to microbubbles, we are compelled to reject this compromise.

Finally, we return to the mesophase model discussed briefly in Sec. I. In the original version of the model proposed in 1983 by Boni, Bilgram, and Kanzig [5] (mesophase I), a homogenous boundary layer with properties intermediate between the liquid and crystal states was proposed in which the compressibility was assumed to be high enough to engender very large thermodynamic fluctuations which caused the observed intense light scattering. There are three serious objections to this model. First, there is no other experimental evidence for such a layer, and computer simulations such as the recent Lennard-Jones molecular-dynamics simulation by Burke, Broughton, and Gilmer [32] indicate that even at growth rates as high as 80 m/s the transition layer never exceeds a thickness of several angstroms. Second, the thickness of such a layer should be expected to either decrease or remain constant with decreasing growth velocity, while the observed thickness is proportional to v_g^{-1}. Third, as noted by Steininger and Bilgram [9], the large correlation lengths ξ deduced from their $I(\theta)$ measurments are inconsistent with the $\Gamma \propto q^2$ behavior found in the correlation experiments.

The revised mesophase model proposed recently by Steininger and Bilgram [9] (mesophase II) is similarly beset by serious problems. In this model, the intense light scattering is attributed to weakly bound molecular aggregates and Steininger and Bilgram assert that "fluctuations in the index of refraction are...due...to the formation and decay of intermolecular structures." However, for transient scatterers with mean lifetime τ which also undergo Brownian motion, the decay rate Γ should be given by [21, 23]

$$\Gamma = Dq^2 + \tau^{-1}. \tag{4.1}$$

The observation that $\Gamma \propto q^2$ therefore implies that τ is very long, so that the aggregates would have to be essentially permanent. We should therefore expect that such diffusing aggregates would scatter light according to the Mie theory, so the assertion that this model is also consistent with the Ornstein-Zernike dependence for $I(\theta)$, as claimed by Steininger and Bilgram [9], is inconsistent. Furthermore, the appearance of such aggregates in a boundary layer extending for several micrometers into the fluid would presumably result from the undercooling of the liquid. But liquid salol, which is one of the materials in which interfacial light scattering has been studied, can easily be supercooled far below its melting temperature (eventually forming a glass) and no excess scattering in the supercooled melt corresponding to such aggregates has ever been observed.

We are therefore led to conclude that both mesophase models are inconsistent with experimental observations, and that all diffusive interfacial light scattering is most likely due to microbubbles. We are unable to explain why the cyclohexane data of Steininger and Bilgram do not fit the microbubble model predictions, but we find their alternative explanation unconvincing. We recognize

that the microbubble theory is far from complete, but we suggest that the remaining problems should eventually be resolved.

ACKNOWLEDGMENTS

We wish to acknowledge useful conversations and correspondence with J. Bilgram, P. Mazur, J. Keizer, Y. Yeh, J.C. Toledano, J.M. Laherrere, Ya.E. Geguzin, A.A. Chernov, A. Acrivos, O. Martin, and J. Koplik. We also wish to thank R. Graff for performing the mass-spectroscopy measurements, and P. Barber for providing the program used for the Mie calculations. Research at CCNY was supported by the U.S. Department of Energy under Grant No. DE-FG02-84-ER45132. Research at Minas Gerais was supported by the Brazilian agencies Financiadoro de Estudos e Projectos (FINEP) and Conselho Nacional de Desenvolvimento Cientifico e Tecnologico (CNPQ).

[1] H. Guttinger, J.H. Bilgram, E. Serrallach, and W. Kanzig, Helv. Phys. Acta **48**, 399 (1975).
[2] J.H. Bilgram, H. Guttinger, and W. Kanzig, Phys. Rev. Lett. **40**, 1394 (1978).
[3] H. Guttinger, J.H. Bilgram, and W. Kanzig, J. Phys. Chem. Solids **40**, 55 (1979).
[4] B. Zysset, P. Boni, and J.H. Bilgram, Helv. Phys. Acta **54**, 265 (1981).
[5] P. Boni, J.H. Bilgram, and W. Kanzig, Phys. Rev. A **28**, 2953 (1983).
[6] U. Durig, J.H. Bilgram, and W. Kanzig, Phys. Rev. A **30**, 946 (1984).
[7] P.U. Halter, J.H. Bilgram, and W. Kanzig, J. Chem. Phys. **89**, 2622 (1988).
[8] J.H. Bilgram and R. Steininger, J. Cryst. Growth **99**, 30 (1990) (Proc. ICCG-9).
[9] R. Steininger and J.H. Bilgram, J. Cryst. Growth **112**, 203 (1991).
[10] O.N. Mesquita, D.G. Neal, M. Copic, and H.Z. Cummins, Phys. Rev. B **29**, 2846 (1984).
[11] O.N. Mesquita and H.Z. Cummins, Phys.-Chem. Hydrodyn. **5**, 389 (1984).
[12] H.Z. Cummins, G. Livescu, H. Chou, and M.R. Srinivasan, Solid State Commun. **60**, 857 (1986).
[13] G. Livescu, M.R. Srinivasan, H. Chou, H.Z. Cummins, and O. Mesquita, Phys. Rev. A **36**, 2293 (1987).
[14] L. Williams, M.R. Srinivasan, and H.Z. Cummins, Phys. Rev. Lett. **64**, 1526 (1990).
[15] R.A. Brown, J. Keizer, U. Stelger, and Y. Yeh, J. Phys. Chem. **87**, 4135 (1983).
[16] J.P. Vesenka and Y. Yeh, Phys. Rev. A **38**, 5310 (1988).
[17] O.N. Mesquita, L.O. Ladeira, I. Gontijo, A.G. Oliveira, and G.A. Barbosa, Phys. Rev. B **38**, 1550 (1988).
[18] J.M. Laherrere, H. Savary, R. Mellet, and J.C. Toledano, Phys. Rev. A **41**, 1142 (1990).
[19] J.M. Laherrere, R. Mellet, H. Savary, C. Licoppe, J.F. Scott, and J.C. Toledano, Phys. Rev. A **42**, 3634 (1990).
[20] H.Z. Cummins and L.M. Williams, in *Light Scattering by Liquid Surfaces*, edited by D. Langevin (Dekker, New York, 1992), p. 287.
[21] J. Keizer, P. Mazur, and T. Morita, Phys. Rev. A **32**, 2944 (1985).
[22] W.H. van Saarloos and G.H. Gilmer, Phys. Rev. B **33**, 4927 (1986).
[23] P. Mazur and J. Keizer, Phys. Rev. A **38**, 5267 (1988).
[24] R. Pohl, J. Appl. Phys. **25**, 1170 (1954).
[25] P.S. Epstein and M.S. Plesset, J. Chem. Phys. **18**, 1505 (1950).
[26] W.R. Wilcox and V.H.S. Kuo, J. Cryst. Growth **19**, 221 (1973).
[27] M. Blander and J.L. Katz, AIChE. J. **21**, 833 (1975).
[28] Ya.E. Geguzin and A.S. Dzuba, J. Cryst. Growth **52**, 337 (1981).
[29] E.A. Hemmingsen, J. Appl. Phys. **46**, 213 (1975); Nature **267**, 141 (1977).
[30] W.A. Gerth and E.A. Hemmingsen, J. Colloid Interface Sci. **74**, 80 (1980).
[31] G.H. Gilmer (private communication).
[32] E. Burke, J.Q. Broughton, and G.H. Gilmer, J. Chem. Phys. **89**, 1030 (1988).